High-Entropy Alloys as a Discovery Platform for Electrocatalysis

Batchelor, Thomas A.A.; Pedersen, Jack K.; Winther, Simon H.; Castelli, Ivano E.; Jacobsen, Karsten W.; Rossmeisl, Jan

Published in:
Joule

Link to article, DOI:
10.1016/j.joule.2018.12.015

Publication date:
2019

Document Version
Peer reviewed version

High Entropy Alloys as a Discovery Platform for Electrocatalysis

Thomas A. A. Batchelor[1], Jack K. Pedersen[1], Simon H. Winther[1], Ivano E. Castelli[2], Karsten W. Jacobsen[2], and Jan Rossmeisl[1]

[1] *Department of Chemistry, H.C. Ørsted Building D, Copenhagen University, DK-2100, Copenhagen, Denmark*
[2] *Department of Physics, Building 307, Technical University of Denmark, DK-2800, Lyngby, Denmark*

November 2, 2018

Abstract

High-entropy alloys (HEAs) provide a near-continuous distribution of adsorption energies. This can increase overall catalytic activity since a minority of sites having optimal properties dominate the catalysis. In this report we focus on the oxygen reduction reaction (ORR), where we present the results of density functional theory (DFT) calculated *OH and *O adsorption energies on a random subset of the available binding sites on the surface of HEA IrPdPtRhRu. A simple machine learning algorithm was used to predict the remaining distribution of adsorption energies. We found very good agreement between DFT calculated and predicted values. With a full catalog of available binding sites and corresponding adsorption energies an appropriate expression for predicting catalytic activity was used to optimise the HEA composition by maximising the probability of finding optimal sites. The HEA then becomes a design platform for the unbiased discovery of new alloys by focusing on these sites with exceptional catalytic activity. Setting different optimisation constraints led to a new HEA composition and a binary alloy IrPt, demonstrating significant enhancements over pure Pt(111).

Computational methods have provided the means to better understand catalytic processes and direct catalytic design [1–3]. A result of this is that the adsorption energy of molecules and intermediates on the surface of heterogeneous catalysts has been uncovered as a good descriptor for catalytic activity. These adsorption energies can be tuned by alloying and thereby improve the catalytic activity compared to pure elements [4–9]. In this paper we introduce a methodology for calculating adsorption energies on a class of complex alloys, namely HEAs, which may be defined as near-equimolar alloys of five or more elements [10–12]. Such alloys were first discovered in 2004, but have drawn interest as catalytic materials only in the past couple of years [11, 12]. Research on HEAs in this field has been solely focused on experimental tests of HEAs [13–15].

Our motivation behind investigating HEAs for use as a catalyst comes directly from the inherent surface complexity. HEAs can provide a surface with a very large number of unique binding site environments which will lead to a near-continuum distribution of associated adsorption energies. Within this distribution, sites with optimal properties will dominate the catalytic activity in the same way that steps and microstrain on surfaces can provide the most vital sites on a catalyst [16, 17]. If the composition of the HEA is tuned to obtain a large number of sites with optimal adsorption energies the activity will increase further.

Adsorption on an HEA surface is complex due to the vast number of possible surface sites, making a full description difficult. Known approximate methods for relating surface structure with adsorption energy are already established, namely the d-band model presented by Hammer and Nørskov [18], the generalised coordination number model presented by Calle-Vallejo and co-workers [19],the bonding contribution model proposed by Wang and Hu [20], and the Orbitalwise coordination number model proposed by Xin and Ma [21]. However, none of these models can easily be extended to the multicomponent surface of an HEA. We circumvent this issue by developing a new simple model that predicts adsorption energies due to the composition of the local binding site. This method vastly reduces computation time and allows for the fast estimation of adsorption energies on the millions of available sites.

In this work we focus on the application of an HEA for pushing the boundaries of catalytic activity for the ORR. If reaction intermediates *OH and *O are too stable on the surface they will limit the potential of the reaction and, similarly, if the molecules are not stable enough the reaction will also be limited. In Sabatier volcano plots reaction rates reach a maximum at an optimum adsorption energy, ΔE_{opt}. Pt(111) is the best pure metal surface for the ORR, however the adsorption of *OH is ~ 0.1 eV too strong [22]. Finding an HEA surface comprised of enough binding sites with near-perfect adsorption energies may provide a simple means of surpassing the activity of pure Pt.

The HEA under consideration in this work is IrPdPtRhRu. These constituent elements are chosen because their similar atomic radii and low heat of formation make them likely to form a stable HEA (see supplementary information (SI) section S1 for full details), and because the standard electrode potentials for all elements are high which reduces the likelihood of oxidation of the alloy. We establish the stability theoretically in the following section and have found examples of similar HEAs having been successfully synthesised [13,15,24], and show promising catalytic properties.

IrPdPtRhRu stability: The stability of an HEA is maintained by the high level of disorder existing in the distribution of elements throughout the simple crystal structure [25], maximising entropy which in turn minimises free energy. Finding out on a theoretical level whether or not an HEA can form a stable solid solution requires the calculation of a few thermodynamic

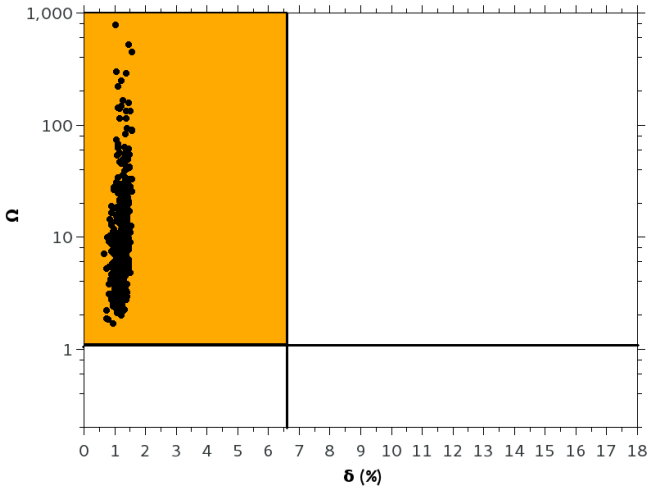

Figure 1: A graph of omega values vs delta values for each 8-atom bulk HEA unit cell. The distribution of data shown is well within the theoretical solid solution requirements of $\delta \leq 6.6\%$ and $\Omega \geq 1.1$ [23]

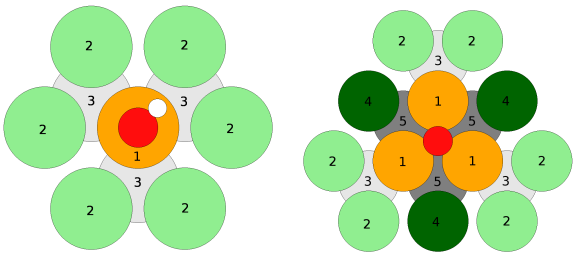

(a) *OH on-top binding **(b)** *O fcc hollow site binding

Figure 2: Schematic showing the way the surface configurations are parametrized to characterize the binding sites using the nearest surface and subsurface elements. Each colored zone represents a set of 5 parameters, except zone 1 for hollow site binding for which the set is 35 parameters. Orange (1): binding site. Light green (2): surface neighbours coordinating once to the binding site. Light grey (3): subsurface neighbours coordinating once to the binding site. Dark green (4): surface neighbours coordinating twice to the binding site. Dark grey (5): subsurface neighbours coordinating twice to the binding site.

properties using details such as the atomic radius, differences in bulk energies and the percentage contribution of the elemental constituents. Researchers have already investigated HEA stability in order to find some simple parameters that form limits on the requirements for stability. These parameters involve the ratio of formation enthalpy to entropy, and the differences in atomic radii [23, 26]. The Hume-Ruthery rules [27] suggest two such parameters that balance these requirements and form the limiting values required for stable HEA formation. The parameters are the atomic radius difference factor, δ, and the ratio taken from the Gibbs free energy of mixing, Ω. Descriptions of these factors are found in SI section S1.

The most reliable way to test stability would be to generate and relax a structure containing a large number of atoms in a crystal lattice. Performing a simulation of such a large structure was not possible, however, due to the computational intensity of ab initio calculations with many atoms. Rather than performing one large simulation we simulated many small fcc unit cells, in this case consisting of 8 atoms, and including periodic boundaries in x,y and z directions. The unit cells were populated by allocating a random choice from the constituent elements to each lattice position. The lattice parameter, a, used in creating the HEA unit cells throughout this thesis was calculated by taking the average value over the pure bulk lattice parameters (found in SI section S9) for the five constituents [28], which is a good approximation according to Vegard's law. We use the average bulk value in all unit cell simulations that follow since the lattice parameter is determined on a longer length scale than a unique local unit cell.

An issue with using such small bulk unit cells for HEAs is that cells are replicated in all directions due to periodic boundary conditions, introducing symmetry in the bulk which no longer resembles a true solid solution HEA. However, these issues are not possible to solve given the aforementioned limits on computation time and power. Therefore 500 unit cells were generated using this method in an attempt to capture a wide range of the possible local environments found in a bulk HEA. Values for δ and Ω were calculated for each unit cell.

We decided it was enough to verify that the values Ω and δ are, respectively, larger than 1.1 and smaller than 6.6% for each structure. If any unit cell does not match this requirement then there is a chance that instability in the lattice structure would prevent the formation of a single solid solution.

The values obtained for Ω and δ are plotted in figure 1. All compositions fall within the δ and Ω bounds, suggesting a great likelihood for the formation of a single solid solution. We find our prediction to be backed up by Hu and co-workers, [15] who have synthesized solid solution HEA nanoparticles with a very similar composition and find them to be stable in both standard and reactive conditions. This is contrary to other Pt alloys, e.g. $PT_3X, (X = Ni, ...)$ where X is both very different in size, and also often with a different lattice structure from Pt leading to intermetallic phases.

Having confirmed the HEA solid solution stability we address the possibility of segregation occurring at the surface. With this in mind 50 4-layered 3x4 slabs were relaxed, where the positions of atoms comprising the top 2 layers were permuted (details found in SI section S2). The energy difference between the 50 slabs remains within 0.03 eV/atom leading us to conclude that the surface will not experience a strong driving force towards surface segregation in vacuum. Regarding adsorbate induced surface segregation, any alloy is expected to show meta-stability, inlcuding Pt_3X alloys, and so in reality surface segregation will occur similar to other alloys.

With the theoretical stability of the HEA now verified we move on to developing a methodology for calculating adsorption energies of OH and O on the HEA surface. A model for predicting adsorption on the HEA is the first step in this methodology. Using the HEA adsorption energy predictions further optimizations are made on the composition of the alloy, such that the alloy serves as a platform from which other new alloys may be discovered. The HEA then represents both a potential new alloy for the ORR and a discovery platform for new catalysts.

Results and Discussion: *OH and *O adsorbates were placed on on-top and fcc hollow binding sites respectively and the adsorption energies calculated with DFT. Since we cannot calculate the full set of adsorption energies we construct a model

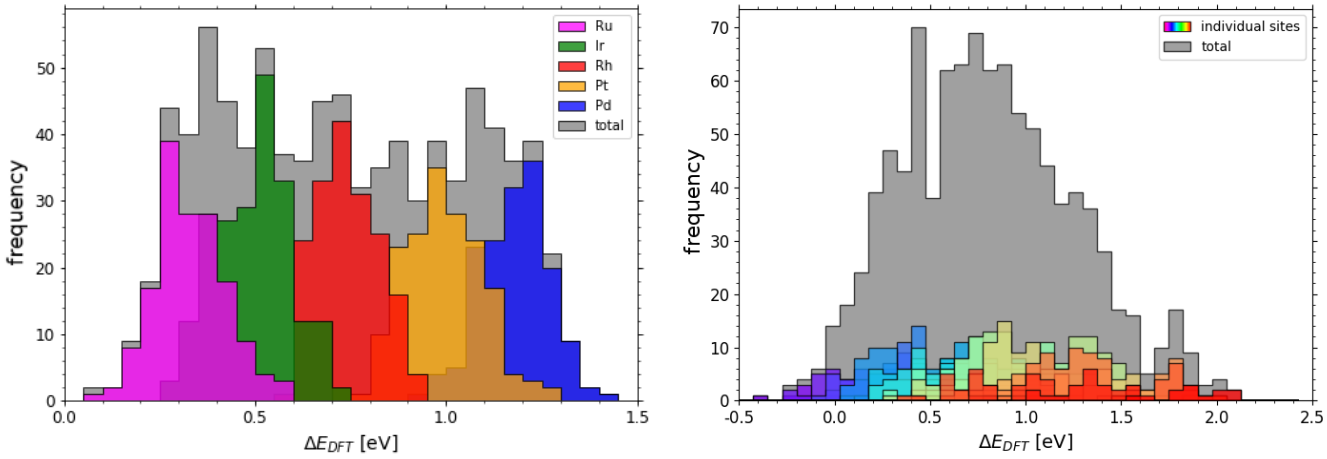

(a) Histogram of 871 DFT calculated *OH adsorption energies. **(b)** Histogram of 998 DFT calculated *O adsorption energies.

Figure 3: Histograms showing the DFT calculated adsorption energies of **(a)** *OH and **(b)** O* on 871 and 998 2x2 periodic unit cells, respectively. Each colour represents an individual on-top or fcc hollow binding site where there exists 5 distinct sites for *OH adsorbed on 1 atom, and 35 for O* adsorbed on a 3-atom ensemble. The binding sites represented by each colour are shown as zone 1 in figure 2.

to link the local atomic environment around the atom(s) with which the adsorbate binds to the adsorption energy using the following linear relationship in the case of an on-top site.

$$\Delta E^i_{pred} = \sum_k^{metals} C_{1,k} N^i_{1,k} + \sum_k^{metals} C_{2,k} N^i_{2,k} + \sum_k^{metals} C_{3,k} N^i_{3,k} \tag{1}$$

Here $C_{1,k}$, $C_{2,k}$ and $C_{3,k}$ are the model parameters and $N^i_{1,k}$, $N^i_{2,k}$ and $N^i_{3,k}$ are the numbers of each element, k, found in each zone numbered 1 through 3 according to the surface configurations in figure 2a. In the case of the hollow site, the first term is modified to run over all the 35 possibilities where 3 metal atoms are binding. Furthermore, two additional zones 4 and 5 are introduced as shown in figure 2b. In this form the model is able to predict all possible surface sites based on counting the nearest neighbours. We discuss the effect of permuting the location of elements with the zones in SI S5, finding that these permutations only lead to adsorption energy perturbations of up to 0.1 eV. The generalized coordination number [19,29] and orbitalwise coordination number [21] methodologies are able to predict binding energies by counting nearest neighbours in a similar way and while they are powerful they remain restricted to different facets of pure metal, or well organised alloy surfaces. These cannot be applied to HEAs due to inherent structural disorder, and since we only consider one facet (fcc111) the generalized coordination number is the same for all sites.

To simulate the randomness of an HEA, DFT calculations were performed on the binding of *OH and *O to 871 and 998 different 2x2 unit cells (see figure S1) respectively, and the resulting adsorption energies are depicted in figures 3a and 3b. Using this data we train our model using the ordinary least squares algorithm [30] with the intention of predicting the full span of available adsorption energies on the HEA surface. We test the model on a set of 3x4 unit cells possessing no symmetry in the modeled surface sites. A comparison between DFT calculated adsorption energies and model predictions are shown in figures 4a and 4b for *OH and *O respectively. The accuracy of these predictions is apparently high, with an RMSD of 0.063 and 0.076 eV for *OH and *O respectively. While these are accurate predictions when compared with DFT, the DFT calculated adsorption energies should have a similar error relative to true adsorption energies so we have seemingly reached the maximum accuracy possible. In order to calculate the uncertainty of an adsorption energy we do calculations with the Bayesian Error Estimation Functional (BEEF), specifically BEEF-vdW which includes a van der Waals correction. Here 2000 calculations are performed per structure using different functionals. With such an ensemble of energies it is trivial to calculate an average and associated error estimate. We find (as seen in SI section S3) that the *OH adsorption energies on 20 HEA slabs, using *OH adsorption on pure Pt(111) as a reference, are accurate when using RPBE compared to the BEEF ensemble average. The error calculated for each adsorption energy difference, in this case taken as the standard deviation of the ensemble, is shown to up to around 0.1 eV.

That such a simple model is able to accurately predict adsorption energies on the complex HEA surface can be easily explained. We posit that the accuracy of the model stems from the idea that the interaction of the nearest-neighbour (NN) atoms with the binding site atoms in zone 1 in figure 2 tends towards a mean-field effect; when viewed as a perturbation to the adsorption energy that the perturbation strength becomes mean-field because the atoms coordinated with each NN tends to the average composition of the HEA. Therefore the interaction strength is also an average and the specific atom locations are of less importance, though non-negligible as discussed in SI S4.

The model is then applied to the full span of available adsorption energies with the predicted distributions being displayed on a histogram, shown in figure 5a for *OH and figure 5b for *O. It is clear that the fully spanned adsorption energies accurately represent the DFT calculated distributions of adsorption energies found in figures 3a and 3b. With the full distribution spanned out we optimise the surface so that the likelihood of finding specific binding sites with the desired adsorption energy is maximised. With this in mind a measure of catalytic activity

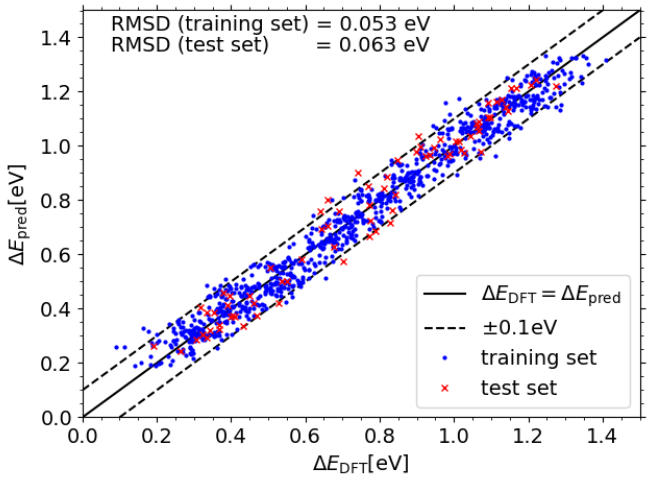

(a) DFT vs predicted *OH adsorption energies.

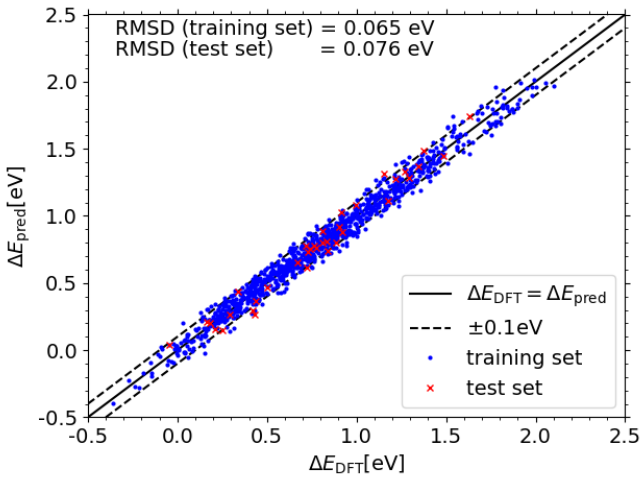

(b) DFT vs predicted *O adsorption energies.

Figure 4: Predicted adsorption energies plotted against DFT calculated energies for **(a)** *OH and **(b)** *O using linear regression. The linear model is trained on **(a)** 871 and **(b)** 998 symmetric 2x2 unit cells (blue dots) and tested on **(a)** 76 and **(b)** 36 asymmetric 3x4 unit cells (red crosses). The linear model uses **(a)** 15 and **(b)** 55 parameters. The dashed lines span the region ±0.1 eV where most of the data is seen to be contained.

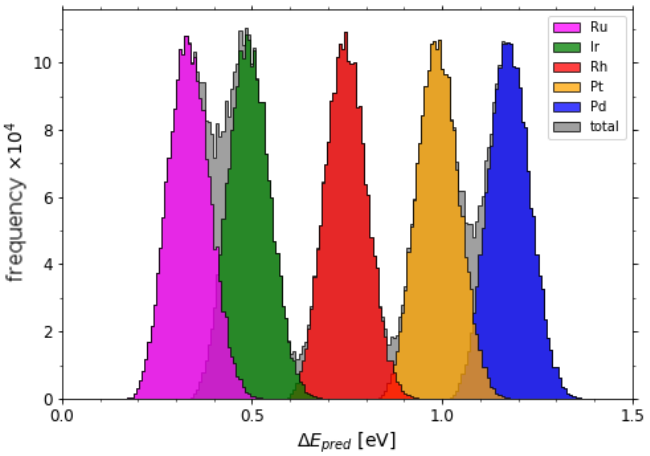

(a) Histogram of full span of predicted energies for *OH.

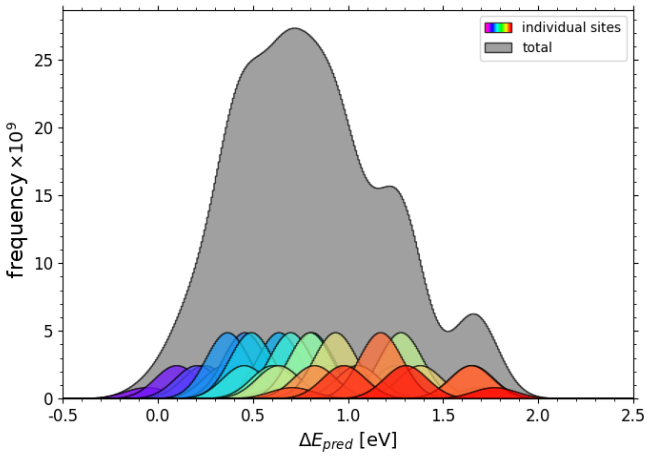

(b) Histogram of full span of predicted energies for *O.

Figure 5: Histograms showing the full span of predicted adsorption energies for **(a)** *OH and **(b)** O* obtained using equation 1. Each colour represents an individual on-top or fcc hollow binding site for *OH and O*, respectively, as in figure 3.

is employed, using the following expressions to determine the activity, A, based on the Sabatier volcano.

$$A = \sum_{i=1}^{Z} \left(\prod_{k}^{metals} f_k^{n_{ik}} \right) \exp\left(-\frac{|\Delta E_i - \Delta E_{opt}|}{k_b T} \right) \qquad (2)$$

Here Z is the total number of surface configurations, ΔE_i is the modeled adsorption energy for the ith surface configuration, ΔE_{opt} is the optimum adsorption energy according to the Sabatier principal, k_b is Boltzmann's constant, T is the absolute temperature, f_k is the atomic fraction of element k, and n_{ik} is the number of element k in the surface configuration i. We use a non-linear optimization method, Sequential Least Squares Programming (SLSQP) [31] and apply many random initial conditions for the algorithm, in order to find the atomic fractions f_k, that maximise the activity in equation 2 at $T = 300$ K. While the focus is placed on *OH adsorption for the composition optimisation since it governs the rate of the limiting steps in the ORR [32,33], this methodology could be applied for the optimisation of more than one adsorption energy.

In order to find a valid comparison for the catalytic activity we apply equation 2 to *OH adsorption on a DFT optimised pure Pt(111) surface, yielding an adsorption energy of 1.0 eV. Since the optimal adsorption energy of *OH is ~ 0.1 eV higher than on Pt(111), we set the value of ΔE_{opt} to 1.1 eV [33], resulting in an activity of $A_{Pt} = 0.021$.

We also don't expect co-adsorbate interactions to be problematic on the surface in this case since the formation of ice-like hexagonal water molecule rings (as is seen on binary alloys [34] and pure Pt(111) [35]) prevent *OH from binding to

neighbouring sites. Changes to adsorption energies on the alloy surface due to water interactions are assumed to be the same as on Pt(111). Since we only consider the activity enhancement relative to Pt(111) the water interaction has no effect on the activity enhancement.

Comparing the activity of pure platinum with that of $Ir_{20}Pd_{20}Pt_{20}Rh_{20}Ru_{20}$ ($A = 0.046$, figure 6a), we find that the activity is doubled and the overpotential is reduced by $e\Delta U = ek_bT\ln(A/A_Pt) = 0.02$ V. Optimisation of the HEA composition leads to the adsorption energy distribution found in figure 6b with the atomic fractions: $(f_{Ir},f_{Pd},f_{Pt},f_{Rh},f_{Ru}) = (0.102, 0.320, 0.093, 0.196, 0.289)$ and an activity of $A = 0.10$ corresponding to a reduction in overpotential of 0.04 V. This composition will form a stable HEA, according to the stability rules described in SI chapter S1. If, however, the constraints are relaxed to allow conventional alloys, we find the following atomic fractions to globally maximise the activity: $(f_{Ir},f_{Pd},f_{Pt},f_{Rh},f_{Ru}) = (0.175, 0.000, 0.825, 0.000, 0.000)$ with an activity of $A = 0.60$, that is more than 28 times higher than for Pt (figure 6d), corresponding to a reduction in overpotential of 0.09 V. According to Sautet and co-workers, alloy catalysts can demonstrate strong surface segregation or reverse segregation in reactive conditions [36], but this problem of metastability is unavoidable for all such alloys. A Pt-Ir binary alloy has been found experimentally to form a stable alloy [37–39] and while the surface anti-segregation energy [40] is moderate we expect mobility to be slow enough to retain alloy composition at the surface. The existence of this binary alloy is also confirmed by observing the phase diagram of Ir-Pt [41]. There exists a large miscibility gap where the metals would separate into two phases up to 1000 K, but above this temperature they are stabilised as a single random fcc solid solution. With slow mobility after annealing one could expect the random alloy to be metastable.

One can view the change to adsorption energy distributions by comparing the histograms in figure 6. The histograms depict very clearly that the composition of the five metals can be tuned to promote local structures with adsorption energies close to 1.1 eV. While $Ir_{17.5}Pt_{82.5}$ represents the global maximum with no constraints placed on the optimisation, a noteworthy local maximum is the binary alloy $Pd_{81.7}Ru_{18.3}$ with an activity 24 times that of Pt or a 0.08 V reduction in overpotential (figure 6c). We find, however, that this alloy is unable to form a stable binary alloy [40, 42].
The optimisations using our model clearly show that complex alloys with a significant proportion of binding sites with adsorption energies close to 1.1 eV demonstrate a greater activity than pure platinum. However, the detailed behaviour depends on the volcano curve which is unlikely to be ideal in reality [33, 43].

An important approximation that has been applied so far is that the lattice parameter has not been optimised, instead being fixed at the average value of the constituent elements (see table S4 for details). However, the optimal compositions found are expected to be influenced by the lattice strain. Calculations of the adjustments to the optimised activities according to a strain correction on the *OH adsorption energy [7]can be found in SI chapter S9.The difference in lattice constant between equal composition HEA and the optimised HEA is small enough that the change in adsorption energy is negligible, according to the strain correction. Re-optimising the composition

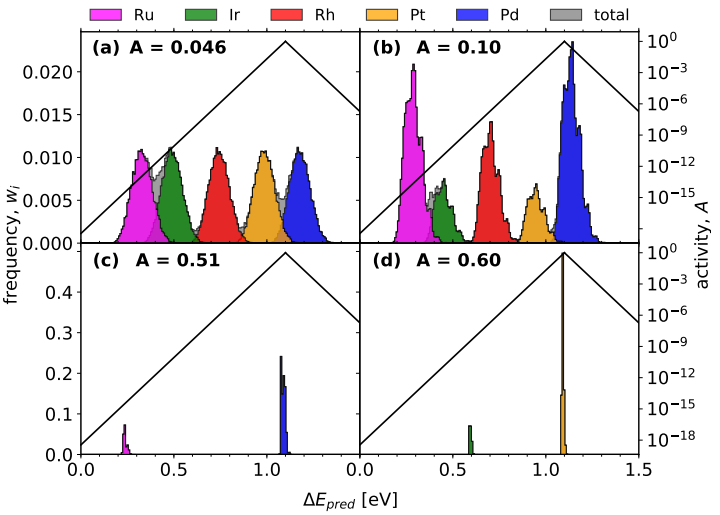

Figure 6: Re-engineered compositions of HEA IrPdPtRhRu showing increasing activity (using equation 2) as the composition is optimized to give the greatest likelihood for the optimum *OH adsorption energy of 1.1 eV. **(a)** $Ir_{20}Pd_{20}Pt_{20}Rh_{20}Ru_{20}$, **(b)** $Ir_{10.2}Pd_{32.0}Pt_{9.30}Rh_{19.6}Ru_{28.9}$, **(c)** $Pd_{81.7}Ru_{18.3}$, **(d)** $Ir_{17.5}Pt_{82.5}$ (global maximum activity). The black volcano plots refer to the axis on the right, and are plotted using equation 2 for hypothetical surfaces with a single adsorption energy given on the bottom axis.

of $Ir_{17.5}Pt_{82.5}$ with strain-adjusted adsorption energies results in a new optimum composition $Ir_{59.1}Pt_{40.9}$ with an activity of $A = 0.32$ corresponding to a reduction in overpotential of 0.07 V.

Conclusions: We have shown that HEAs are potentially interesting as electrocatalysts for ORR. The surface of an HEA provides a near-continuum of adsorption energies due to many surface configurations and the full set of adsorption energies can be spanned out as predicted by a simple model. It is possible to engineer the surface structure to optimise the catalytic activity of specific reactions. This is done by tuning the bulk composition such that binding sites with adsorption energies close to the peak of the volcano curve have an increased availability. The optimisation of the HEA composition outlined in the present work is applicable to any surface reaction where an adsorption energy of an intermediate is the key descriptor, and the model provides an accurate and time-efficient mapping between adsorption energy and surface structure that is crucial for the success of the optimisation.

Methods: All DFT calculations are performed using GPAW [44, 45], an implementation of the projector augmented-wave (PAW) method in the atomic simulation environment (ASE) [46]. The exchange-correlation functional used is RPBE [47], and the wave functions have been expanded in plane-waves with an energy cutoff of 400 eV. The eigensolver RMM-DIIS (Residual minimization method - direct inversion in iterative subspace) was employed throughout. Stability on bulks were calculated on randomly generated 8 atom unit cells (figure S2) with k-points (x,y,z) = (8,8,4), and adsorption energies used for training were calculated on 2x2, 4-layered slabs (figure S1 (a) and (b)) with k-points (x,y,z) = (4,4,1) while adsorption energies used for testing were calculated on 3x4, 4-layered (48 atoms) slabs (figure S1 (c) and (d)) with k-points (x,y,z) =

(3,3,1). 14 Åof vacuum was added between the periodic unit cells in the z-direction. For all calculations on slabs the two bottom layers were fixed and only the two upper layers were allow to relax during geometry optimisation. Adsorption energies were calculated using the following expressions

$$\Delta E_{OH} = E_{slab+OH} + \frac{1}{2}E_{H_2} - (E_{slab} + E_{H_2O}) \quad (3)$$

and

$$\Delta E_{O} = E_{slab+O} + E_{H_2} - (E_{slab} + E_{H_2O}) \quad (4)$$

where E_{slab+X} is the DFT electronic energy of the slab with X = O or OH adsorbed, E_{H_2} is the elecronic of H_2, E_{slab} is the electronic energy of the slab and E_{H_2O} is the electronic energy of H_2O. For this work we do not include calculations of zero-point energy corrections since the composition optimisations are calculated with relative energies and we would find the same optimum compositions. Molecular energies E_{H_2} and E_{H_2O} were calculated using the same settings as the slabs, but with 18x18x18 Åunit cells, k-points (x,y,z) = (1,1,1), and without periodic boundary conditions. Adsorption energies and relaxed structure geometries for every DFT calculation were stored in a database which can be found at http://nano.ku.dk/english/research/theoretical-electrocatalysis/katladb/orr-on-hea/.

References

[1] Jacobsen, C. J. H. *et al.* Catalyst design by interpolation in the periodic table: bimetallic ammonia synthesis catalysts. *J. Am. Chem. Soc.* **123**, 8404–8405 (2001).

[2] Strasser, P. *et al.* High throughput experimental and theoretical predictive screening of materials a comparative study of search strategies for new fuel cell anode catalysts. *J Phys. Chem. B* **107**, 11013–11021 (2003).

[3] Alayoglu, S., U Nilekar, A., Mavrikakis, M. & Eichhorn, B. Rupt coreshell nanoparticles for preferential oxidation of carbon monoxide in hydrogen. *Nat. Mater.* **7**, 333–8 (2008).

[4] Greeley, J. *et al.* Alloys of platinum and early transition metals as oxygen reduction electrocatalysts. *Nat. Chem.* **1**, 552–6 (2009).

[5] Lin, S.-P., Wang, K.-W., Liu, C.-W., Chen, H.-S. & Wang, J.-H. Trends of oxygen reduction reaction on platinum alloys: A computational and experimental study. *J. Phys. Chem. B* **119**, 15224–15231 (2015).

[6] Stamenkovic, V. R. *et al.* Improved oxygen reduction activity on $Pt_3Ni(111)$ via increased surface site availability. *Science* **315**, 493–497 (2007).

[7] Escudero-Escribano, M. *et al.* Tuning the activity of Pt alloy electrocatalysts by means of the lanthanide contraction. *Science* **352**, 73–76 (2016). URL http://science.sciencemag.org/content/352/6281/73. http://science.sciencemag.org/content/352/6281/73.full.pdf.

[8] Jensen, K. D. *et al.* Elucidation of the oxygen reduction volcano in alkaline media using a copper-platinum(111) alloy. *Angew. Chem. Int. Edit.* **57**, 2800–2805 (2018). URL http://dx.doi.org/10.1002/anie.201711858.

[9] Brimaud, S., Engstfeld, A. K., Alves, O. B., Hoster, H. E. & Behm, R. J. Oxygen reduction on structurally well defined, bimetallic ptru surfaces: Monolayer ptxru1x/ru(0001) surface alloys versus pt film covered ru(0001). *Top. Catal.* **57**, 222–235 (2014).

[10] Miracle, D. & Senkov, O. A critical review of high entropy alloys and related concepts. *Acta Mater.* **122**, 448 – 511 (2017). URL http://www.sciencedirect.com/science/article/pii/S1359645416306759.

[11] Yeh, J.-W. *et al.* Nanostructured high-entropy alloys with multiple principal elements: Novel alloy design concepts and outcomes. *Adv. Eng. Mater.* **6**, 299–303 (2004).

[12] Cantor, B., Chang, I., Knight, P. & Vincent, A. Microstructural development in equiatomic multicomponent alloys. *Mater. Sci. Eng. A* **375-377**, 213 – 218 (2004).

[13] Yusenko, K. V. *et al.* First hexagonal close packed high-entropy alloy with outstanding stability under extreme conditions and electrocatalytic activity for methanol oxidation. *Scripta Mater.* **138**, 22 – 27 (2017). URL http://www.sciencedirect.com/science/article/pii/S135964621730266X.

[14] Y. Lv, Z. *et al.* Development of a novel high-entropy alloy with eminent efficiency of degrading azo dye solutions. *Sci. Rep.* **6**, 34213 (2016).

[15] Yao, Y. *et al.* Carbothermal shock synthesis of high-entropy-alloy nanoparticles. *Science* **359**, 1489–1494 (2018).

[16] Dahl, S. *et al.* Role of steps in N_2 activation on Ru(0001). *Phys. Rev. Lett.* **83**, 1814–1817 (1999).

[17] Olivier, L. B. *et al.* Effect of atomic vacancies on the structure and the electrocatalytic activity of ptrich/c nanoparticles: A combined experimental and density functional theory study. *ChemCatChem* **9**, 2324–2338 (2017). URL https://onlinelibrary.wiley.com/doi/abs/10.1002/cctc.201601672.

[18] Hammer, B. & Nørskov, J. Theoretical surface science and catalysiscalculations and concepts. In *Impact of Surface Science on Catalysis*, vol. 45 of *Advances in Catalysis*, 71 – 129 (Academic Press, 2000). URL http://www.sciencedirect.com/science/article/pii/S0360056402450134.

[19] Calle-Vallejo, F., Loffreda, D., Koper, M. & Sautet, P. Introducing structural sensitivity into adsorptionenergy scaling relations by means of coordination numbers. *Nat. Chem.* **7**, 403–410 (2015).

[20] Wang, Z. & Hu, P. Formulating the bonding contribution equation in heterogeneous catalysis: a quantitative description between the surface structure and adsorption energy. *Phys. Chem. Chem. Phys.* **19**, 5063–5069 (2017). URL http://dx.doi.org/10.1039/C6CP08493A.

[21] Ma, X. & Xin, H. Orbitalwise coordination number for predicting adsorption properties of metal nanocatalysts. *Phys. Rev. Lett.* **118**, 036101 (2017). URL https://link.aps.org/doi/10.1103/PhysRevLett.118.036101.

[22] Nørskov, J. K. *et al.* Origin of the overpotential for oxygen reduction at a fuel-cell cathode. *J. Phys. Chem. B* **108**, 17886–17892 (2004). URL https://doi.org/10.1021/jp047349j. https://doi.org/10.1021/jp047349j.

[23] Yang, X. & Zhang, Y. Prediction of high-entropy stabilized solid-solution in multi-component alloys. *Mater. Chem. Phys.* **132**, 233 – 238 (2012).

[24] Chen, X. *et al.* Multi-component nanoporous platinumrutheniumcopperosmiumiridium alloy with enhanced electrocatalytic activity towards methanol oxidation and oxygen reduction. *Journal of Power Sources* **273**, 324 – 332 (2015).

[25] Wang, W. R. *et al.* Effects of al addition on the microstructure and mechanical property of AlxCoCrFeNi high-entropy alloys. *Intermetallics* **26**, 44–51 (2012).

[26] Zhang, Y., Zhou, Y., Lin, J., Chen, G. & Liaw, P. Solid-solution phase formation rules for multi-component alloys. *Adv. Eng. Mater.* **10**, 534–538 (2008).

[27] Mizutani, U. *Hume-Rothery Rules for Structurally Complex Alloy Phases* (CRC Press, 2010).

[28] Colinet, C. Ab-initio calculation of enthalpies of formation of intermetallic compounds and enthalpies of mixing of solid solutions. *Intermetallics* **11**, 1095 – 1102 (2003).

[29] Calle-Vallejo, F. *et al.* Finding optimal surface sites on heterogeneous catalysts by counting nearest neighbors. *Science* **350**, 185–189 (2015).

[30] Abu-Mostafa, Y. S., Magdon-Ismail, M. & Lin, H.-T. *Learning From Data*, 84–87 (AMLBook, 2012).

[31] Kraft, D. A software package for sequential quadratic programming. Tech. Rep., DFVLR-FB 88-28 (1988).

[32] Rossmeisl, J., Karlberg, G. S., Jaramillo, T. & Nørskov, J. K. Steady state oxygen reduction and cyclic voltammetry. *Faraday Discuss.* **140**, 337–346 (2009). URL http://dx.doi.org/10.1039/B802129E.

[33] Stephens, I. E. L., Bondarenko, A. S., Grønbjerg, U., Rossmeisl, J. & Chorkendorff, I. Understanding the electrocatalysis of oxygen reduction on platinum and its alloys. *Energy Environ. Sci.* **5**, 6744–6762 (2012). URL http://dx.doi.org/10.1039/C2EE03590A.

[34] Fischer, J. M., Mahlberg, D., Roman, T. & Groß, A. Water adsorption on bimetallic ptru/pt(111) surface alloys. *Proceedings of the Royal Society of London A: Mathematical, Physical and Engineering Sciences* **472** (2016).

[35] Hodgson, A. & Haq, S. Water adsorption and the wetting of metal surfaces. *Surface Science Reports* **64**, 381 – 451 (2009).

[36] Vignola, E. *et al.* Acetylene adsorption on pdag alloys: Evidence for limited island formation and strong reverse segregation from monte

carlo simulations. *The Journal of Physical Chemistry C* **122**, 15456–15463 (2018).
[37] Bunce, N. J. & Bejan, D. Mechanism of electrochemical oxidation of ammonia. *Electrochim. Acta* **56**, 8085 – 8093 (2011).
[38] de Mishima, B., Lescano, D., Holgado, T. & Mishima, H. Electrochemical oxidation of ammonia in alkaline solutions: its application to an amperometric sensor. *Electrochim. Acta* **43**, 395 – 404 (1998).
[39] Zhong, C., Hu, W. B. & Cheng, Y. F. Recent advances in electrocatalysts for electro-oxidation of ammonia. *J. Mater. Chem. A* **1**, 3216–3238 (2013).
[40] Ruban, A., Skriver, H. & Nørskov, J. Surface segregation energies in transition-metal alloys. *Phys. Rev. B* **59**, 15990–16000 (1999).
[41] Franke, P. & Neuschütz, D. *Ir-Pt (Iridium - Platinum): Datasheet from Landolt-Börnstein - Group IV Physical Chemistry · Volume 19B5: "Binary Systems. Part 5: Binary Systems Supplement 1" in SpringerMaterials* (Springer-Verlag Berlin Heidelberg, 2007). URL https://materials.springer.com/lb/docs/sm_lbs_978-3-540-45280-5_80.
[42] Wu, D., Kusada, K. & Kitagawa, H. Recent progress in the structure control of pdru bimetallic nanomaterials. *Sci. Technol. Adv. Mat.* **17**, 583–596 (2016).
[43] Deshpande, S., Kitchin, J. R. & Viswanathan, V. Quantifying uncertainty in activity volcano relationships for oxygen reduction reaction. *ACS Catal.* **6**, 5251–5259 (2016). URL https://doi.org/10.1021/acscatal.6b00509.
[44] Mortensen, J. J., Hansen, L. B. & Jacobsen, K. W. Real-space grid implementation of the projector augmented wave method. *Phys. Rev. B* **71**, 035109 (2005).
[45] Enkovaara, J. *et al.* Electronic structure calculations with gpaw: a real-space implementation of the projector augmented-wave method. *J. Phys. Condens. Mat.* **22**, 253202 (2010). URL http://stacks.iop.org/0953-8984/22/i=25/a=253202.
[46] Larsen, A. H. *et al.* The atomic simulation environment - a python library for working with atoms. *J. Phys. Condens. Mat.* **29**, 273002 (2017). URL http://stacks.iop.org/0953-8984/29/i=27/a=273002.
[47] Hammer, B., Hansen, L. B. & Nørskov, J. K. Improved adsorption energetics within density-functional theory using revised Perdew-Burke-Ernzerhof functionals. *Phys. Rev. B* **59**, 7413–7421 (1999).

Acknowledgements
We acknowledge support from research grant 9455 from VILLUM FONDEN, the Carlsberg Foundation (grant CF15-0165) and the Innovation Fund Denmark (grand solution ProActivE 5124-00003A).
Author contributions
T. Batchelor designed and set up the DFT calculations. All authors contributed to the development of the model, discussion of the results and to the writing of the manuscript.
Additional information
Supplementary information is available online at http://nano.ku.dk/english/research/theoretical-electrocatalysis/katladb/orr-on-hea/. Correspondence and extra material requests should be addressed to T. Batchelor and J. Rossmeisl.
Competing interests
All authors declare no competing interests.